

## RPA analysis of a two-orbital model for the BiS<sub>2</sub>-based superconductors

G. B. Martins,<sup>1,\*</sup> A. Moreo,<sup>2</sup> and E. Dagotto<sup>2</sup>

<sup>1</sup>*Department of Physics, Oakland University, Rochester, Michigan 48309, USA*

<sup>2</sup>*Department of Physics and Astronomy, University of Tennessee, Knoxville, Tennessee 37996, USA and Materials Science and Technology Division, Oak Ridge National Laboratory, Oak Ridge, Tennessee 37831, USA*

(Received 1 December 2012; revised manuscript received 4 January 2013; published 8 February 2013)

The random-phase approximation (RPA) is here applied to a two-orbital model for the BiS<sub>2</sub>-based superconductors that was recently proposed by Usui *et al.* [*Phys. Rev. B* **86**, 220501(R) (2012)]. Varying the density of doped electrons per Bi site  $n$  in the range  $0.46 \leq n \leq 1.0$ , the spin fluctuations promote competing  $A_{1g}$  and  $B_{2g}$  superconducting states with similar pairing strengths, in analogy with the  $A_{1g}$ - $B_{1g}$  near degeneracy found also within RPA in models for pnictides. At these band fillings, two hole pockets centered at  $(0,0)$  and  $(\pi,\pi)$  display nearly parallel Fermi-surface segments close to wave vector  $(\pi/2,\pi/2)$ , whose distance increases with  $n$ . After introducing electronic interactions treated in the RPA, the interpocket nesting of these segments leads to pair scattering with a rather “local” character in  $k$  space. The similarity between the  $A_{1g}$  and  $B_{2g}$  channels observed here should manifest in experiments on BiS<sub>2</sub>-based superconductors if the pairing is caused by spin fluctuations.

DOI: [10.1103/PhysRevB.87.081102](https://doi.org/10.1103/PhysRevB.87.081102)

PACS number(s): 74.20.Mn, 74.20.Rp, 74.70.-b

**Introduction.** The recently discovered family of layered bismuth oxysulfide superconductors<sup>1–22</sup> has immediately attracted considerable attention from the condensed matter community due to its close similarities with the famous iron-pnictide superconductors.<sup>23–27</sup> As in the case of other layered unconventional superconductors, such as the cuprates and the aforementioned iron pnictides/chalcogenides, this new family displays a layered structure involving BiS<sub>2</sub> planes where the observed superconductivity is believed to reside. The first report of superconductivity originated in Bi<sub>4</sub>O<sub>4</sub>S<sub>3</sub>, with  $T_c = 4.5$  K.<sup>1</sup> Superconductivity has also been reported in RO<sub>1-x</sub>F<sub>x</sub>BiS<sub>2</sub>, where  $R = \text{La, Nd, Ce, and Pr}$ , with corresponding  $T_c = 10.6,$ <sup>2</sup>  $5.6,$ <sup>5</sup>  $3.0,$ <sup>15</sup> and  $5.5$  K.<sup>17</sup> These compounds are metallic in the normal state and density functional theory calculations indicate that the relevant bands crossing the Fermi surface (FS) originate mainly from the Bi  $6p$  orbitals, as shown, e.g., for LaO<sub>1-x</sub>F<sub>x</sub>BiS<sub>2</sub>.<sup>3</sup> However, contrary to the majority of the Cu- and Fe-based unconventional superconductors, no magnetically ordered phase has been detected thus far in the BiS<sub>2</sub> compounds. This apparent absence of magnetism in the BiS<sub>2</sub> compounds *may* still locate them in the same category as LiFeAs, FeSe, and possibly Sr<sub>2</sub>VO<sub>3</sub>FeAs,<sup>24</sup> which are also nonmagnetic but their pairing properties are widely believed to still originate in short-range magnetic fluctuations. For these reasons, and despite the absence of observed long-range magnetism in BiS<sub>2</sub>, it is important to study the potential role of spin fluctuations in these novel materials and the pairing channels that those fluctuations tend to favor, to help in the analysis of experimental data. It is important to note that there is experimental support for considering at least Bi<sub>4</sub>O<sub>4</sub>S<sub>3</sub> as an unconventional superconductor (see Ref. 4 for details). Recent theoretical work has interpreted superconductivity as originating from electron-phonon coupling.<sup>11,28</sup> However, subsequent neutron scattering experiments<sup>29</sup> have not given support to this scenario.

In this Rapid Communication, the two-orbital (2-orbital) model recently introduced by Usui *et al.* is adopted.<sup>3</sup> The fact that the relevant orbitals in BiS<sub>2</sub> compounds are  $p$ -type, where

Coulomb interactions should be smaller than in  $d$  orbitals, turns RPA into a suitable technique, whose results deserve a careful analysis if electron correlations are found to be important for superconductivity in these materials. Similar calculations for a related four-orbital model<sup>3</sup> are under way. Note that in Ref. 3 a brief discussion of RPA calculations has already been presented. The results discussed by Usui *et al.* consisted of a single set of couplings (equivalent to our  $J/U = 0.2$  calculations below) at  $n = 0.5$ . Their early weak-coupling RPA analysis is here expanded via a systematic study of the influence of the band filling  $n$  and the identification of the dominant channels for superconductivity under the assumption of a spin fluctuations mechanism. The main contribution of our present effort is the identification of closely competing  $B_{2g}$  and  $A_{1g}$  gap functions as the dominant pairing channels, particularly for band fillings around  $n = 0.5$ . At quarter filling ( $n = 1.0$ ), another pair of almost degenerate gap functions (with symmetries  $A_{2g}$  and  $B_{1g}$ ) is found to closely compete with the previously mentioned dominant pair, especially at  $J/U = 0.3$ .<sup>30</sup>

**Hamiltonian.** The 2-orbital model described by Usui *et al.*<sup>3</sup> contains hopping parameters up to fourth neighbors, and in  $k$  space is given by

$$H_{\text{TB}}(\mathbf{k}) = \sum_{\mathbf{k}, \sigma, \mu, \nu} T^{\mu\nu}(\mathbf{k}) d_{\mathbf{k}, \mu, \sigma}^\dagger d_{\mathbf{k}, \nu, \sigma}, \quad (1)$$

where

$$T^{XX} = 2t_x^X (\cos k_x + \cos k_y) + 2t_{x\mp y}^X \cos(k_x \pm k_y) + 2t_{2x\mp y}^X [\cos(2k_x \pm k_y) + \cos(k_x \pm 2k_y)] + \epsilon_x, \quad (2)$$

$$T^{YY} = 2t_x^Y (\cos k_x + \cos k_y) + 2t_{x\pm y}^Y \cos(k_x \mp k_y) + 2t_{2x\pm y}^Y [\cos(2k_x \mp k_y) + \cos(k_x \mp 2k_y)] + \epsilon_y, \quad (3)$$

$$T^{XY} = T^{YX} = 2t_x^{XY} (\cos k_x - \cos k_y) + 4t_{2x}^{XY} (\cos 2k_x - \cos 2k_y) + 4t_{2x+y}^{XY} (\cos 2k_x \cos k_y - \cos k_x \cos 2k_y). \quad (4)$$

TABLE I. Tight-binding parameters (eV) for 2-orbital model.

$\epsilon_{X,Y}$	$t_x^{X,Y}$	$t_{x\mp y}^{X,Y}$	$t_{x\pm y}^{X,Y}$	$t_{2x\mp y}^{X,Y}$	$t_{2x\pm y}^{X,Y}$	$t_x^{XY}$	$t_{2x}^{XY}$	$t_{2x+y}^{XY}$
2.811	-0.167	0.094	0.880	0.014	0.069	0.107	-0.028	0.020

The operator  $d_{\mathbf{k},\nu,\sigma}^\dagger$  ( $d_{\mathbf{k},\nu,\sigma}$ ) in Eq. (1) creates (annihilates) an electron in band  $\nu = X, Y$ , with spin  $\sigma = \pm$ , and wave vector  $\mathbf{k}$ . The values for the hopping parameters are those from Ref. 3, and are reproduced in Table I for completeness (in eV units, as used throughout this paper). Figure 1(a) shows the FS hole pockets for four different band fillings  $n = 0.46, 0.5, 0.65$ , and  $1.0$ , with corresponding chemical potentials  $\mu = 1.10375, 1.12514, 1.21828$ , and  $1.52621$  (in principle,  $n = x$  in  $\text{LaO}_{1-x}\text{F}_x\text{BiS}_2$ ).<sup>3</sup> Panel (b) shows the corresponding noninteracting magnetic susceptibilities  $\chi_0$ . The leftmost peaks in  $\chi_0$ , located at  $(k_n, 0)$ , with  $0 \lesssim k_n \lesssim \pi/2$  as the filling varies from  $n = 0.46$  to  $1.0$ , can be associated to FS nesting once it is noticed that their position matches the *horizontal* separation between the two adjacent FS segments from the pockets centered at  $(0,0)$  ( $\Gamma$ ) and  $(\pi,\pi)$  ( $M$ ), as highlighted by the dashed box in panel (a) and sketched in the inset to panel (b). Note that the horizontal separation is well defined if the two FS segments are parallel, which is the limiting case as  $n$  increases, as shown in the inset, to  $n = 1.0$  (for details, see Fig. 5 and the associated discussion). It is also important to remark that once interactions are introduced, the leftmost peak in  $\chi_0$  is the one that diverges in the RPA calculation of the *spin* susceptibility  $\chi_{\text{RPA}}$  for almost all the fillings and various values of interaction parameters. This divergence indicates a tendency to magnetic order, or at least strong spin fluctuations (paramagnons), with characteristic wavelength determined by  $(k_n, 0)$ . Our analysis is not extended into the  $n \leq 0.45$  region since there the topology of the FS changes (see Ref. 3 for details of the FS at lower fillings<sup>31</sup>).

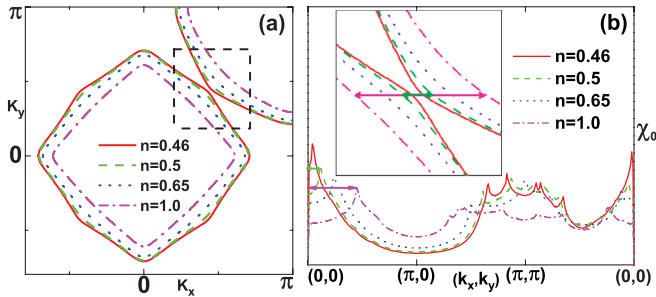


FIG. 1. (Color online) (a) Hole pockets for four different electronic fillings:  $n = 0.46$  (solid red),  $n = 0.50$  (dashed green),  $n = 0.65$  (dotted blue), and  $n = 1.00$  (dot-dashed magenta). Note that close to the  $(\pi/2, \pi/2)$  wave vector, where the  $n = 0.46$  pockets almost touch, the increase of  $n$  decreases the area of the hole pockets and, more importantly, the adjacent FS segments (inside the dashed box) become more and more parallel. (b) Lindhard function  $\chi_0$  for the same fillings as in panel (a). Note that the position in  $k$  space of the leftmost peak is clearly associated to FS nesting through a  $(k_n, 0)$  vector, as indicated in the inset, which zooms in the dashed box in panel (a). Indeed, the position of the leftmost peaks in  $\chi_0$  agree (within a few percent) with the vectors indicated in the inset (see text for details, especially Fig. 5). Obviously, there are additional nesting vectors that become evident in a 2D plot of  $\chi_0$  [Fig. 5(b)].

The Coulomb interaction in the Hamiltonian is given by

$$H_{\text{int}} = U \sum_{i,\alpha} n_{i,\alpha,\uparrow} n_{i,\alpha,\downarrow} + (U' - J/2) \sum_{i,\alpha < \beta} n_{i,\alpha} n_{i,\beta} - 2J \sum_{i,\alpha < \beta} \mathbf{S}_{i,\alpha} \cdot \mathbf{S}_{i,\beta} + J \sum_{i,\alpha < \beta} (d_{i,\alpha,\uparrow}^\dagger d_{i,\alpha,\downarrow}^\dagger d_{i,\beta,\downarrow} d_{i,\beta,\uparrow} + \text{H.c.}), \quad (5)$$

where the notation is standard and the many terms have been described elsewhere.<sup>32</sup> Here, the usual relation  $U' = U - 2J$  is assumed, and  $J/U$  is a parameter. Calculations were done for  $0.1 \leq J/U \leq 0.4$ , in steps of 0.1, for the four fillings  $n = 0.46, 0.50, 0.65$ , and  $1.0$ . The multiorbital RPA calculations performed here follow closely those described in Ref. 33, and previous works by the authors.<sup>32,34</sup> All results were obtained at temperature  $T = 10^{-4}$  and an imaginary part  $\eta = 10^{-5}$  was used to regularize the Green's functions.

Our RPA results for spin-singlet pairing link the dominant superconducting gap functions to spin fluctuations, which originate in FS nesting and are enhanced by electronic interactions. The particular relative topology of the two adjacent hole pockets (see Fig. 1) promotes pairing whose strength is independent of the global symmetry of the pairing functions [see Fig. 4(b)]. Indeed, the  $B_{2g}$  and  $A_{1g}$  symmetries have essentially the same pairing strength, which is determined by pair scattering between these two adjacent FS segments (see Fig. 5) close to  $(\pi/2, \pi/2)$  in the Brillouin zone (BZ). In addition, our results show that both dominant gap functions change sign between these two segments (Figs. 2–4), and the pairing is through the intraorbital scattering channel [Figs. 3(b) and 3(c)]. The near degeneracy  $A_{1g}$ - $B_{2g}$  is the analog of the near degeneracy  $A_{1g}$ - $B_{1g}$  found also in RPA calculations for the pnictides,<sup>33</sup> since the pocket structures in both cases can be related by a  $45^\circ$  rotation. Results for spin-triplet pairing are presented in the Supplemental Material.<sup>35</sup>

**Results and Discussion.** As mentioned above, the most important feature of the FS for fillings between 0.46 and 1.0 is that the hole pockets centered at the  $\Gamma$  and  $M$  points present almost parallel segments close to the  $(\pi/2, \pi/2)$  wave vector, becoming more and more parallel as the pockets shrink, with increasing filling [see Fig. 1(a) and inset in Fig. 1(b)]. In Figs. 2 and 3 it will be shown that this has

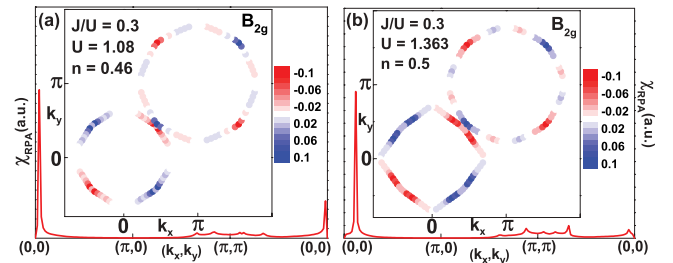


FIG. 2. (Color online) RPA spin susceptibility (solid red curves in the main panels) and dominant gap function (red and blue dots in the insets) for (a)  $n = 0.46$  and (b)  $n = 0.50$ . In the inset to each panel, the dominant gap function with symmetry  $B_{2g}$  is shown. The subdominant gap function (not shown) has symmetry  $A_{1g}$  and its eigenvalue is almost degenerate with the dominant one (see text).

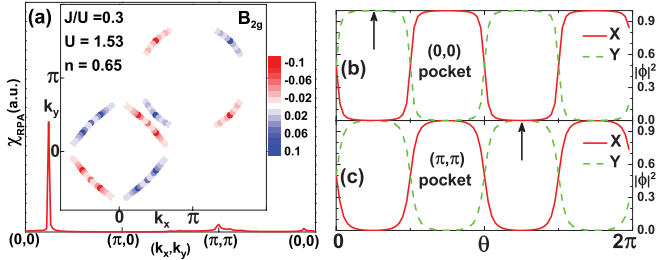


FIG. 3. (Color online) (a) RPA spin susceptibility and dominant gap function for  $n = 0.65$ . Orbital composition for the  $(0,0)$  and  $(\pi,\pi)$  FS pockets ( $n = 0.65$ ), (b) and (c), respectively. The winding angle  $\theta$  runs counterclockwise, starting from the  $k_x$  direction. Assuming the nesting described in the inset to Fig. 1(b) as producing the spin fluctuations that provide pairing, the pair coupling is then intraorbital.

important consequences for the spin fluctuations and the superconducting pairing associated with this 2-orbital model. Indeed, as displayed in the main panel of Fig. 2(a) [solid (red) curve], there is a divergence in the RPA spin susceptibility for very small  $\mathbf{k}$  values:  $\mathbf{k}_{0.46} \sim (\pi/25, 0)$  for  $n = 0.46$ , and  $\mathbf{k}_{0.50} \sim (\pi/8, 0)$  for  $n = 0.50$  [panel (b)]. A divergence in the spin susceptibility  $\chi_{\text{RPA}}$  may point to magnetic order, or at least to strong spin fluctuations with wave vector  $\mathbf{k}_n$ . Figure 3(a) shows the same calculations, but now for  $n = 0.65$ . Note that although  $\chi_0$  displays a broad-peak structure around  $(\pi, \pi)$  [see Fig. 1(b)],  $\chi_{\text{RPA}}$  does not present a divergence in this region. In the insets to Figs. 2(a) and 2(b), and in Fig. 3(a), it is shown that the dominant gap function at the FS has symmetry  $B_{2g}$  for the three cases, showing that despite the changes in the size of the hole pockets the results are qualitatively the same. Figures 3(b) and 3(c) contain the orbital contribution ( $X$ , red solid curve;  $Y$ , green dashed curve) of the BZ states at the FS for the  $\Gamma$  and  $M$  pockets, respectively, indicating intraorbital pairing. It is interesting to note that the modifications in the position of the peak in  $\chi_{\text{RPA}}$  correlates well with the “separation” between the  $\Gamma$  and  $M$  hole pockets in the region around  $(\pi/2, \pi/2)$ . For the purposes of describing our results, this separation will be defined as the *horizontal* distance between two parallel lines

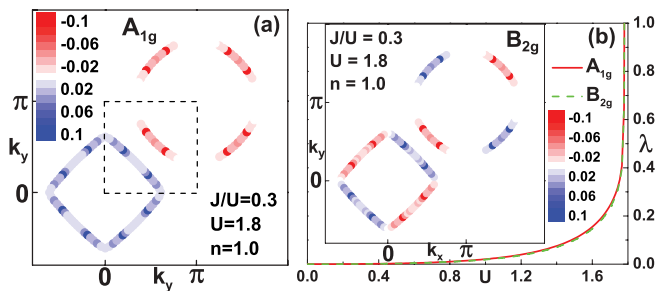


FIG. 4. (Color online) (a) Dominant gap function with symmetry  $A_{1g}$  at  $n = 1.0$ . (b) Main panel: normalized pairing strengths  $\lambda$  for the dominant ( $A_{1g}$ , solid red curve) and subdominant ( $B_{2g}$ , dashed green curve) gap functions. Although the two curves are very close, the eigenvalues are *not* degenerate. In the inset, the structure of the subdominant gap function ( $B_{2g}$ ) is shown. When compared to that of the dominant one [ $A_{1g}$  in panel (a)], it is clear that the structures around  $(\pi/2, \pi/2)$  are very similar to each other, explaining why the pairing strengths (eigenvalues) are the same. The region inside the dashed box in panel (a) is analyzed in detail in Fig. 5(a).

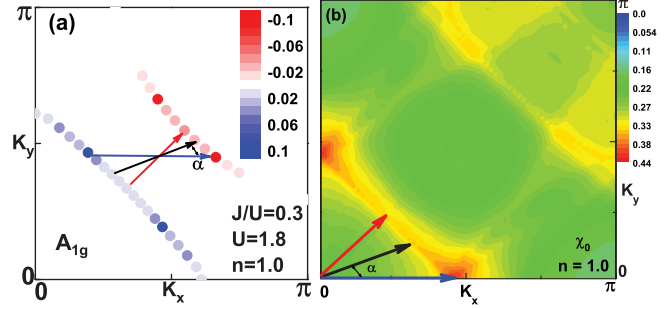


FIG. 5. (Color online) (a) Region around point  $(\pi/2, \pi/2)$  of the BZ [dashed box in Fig. 4(a)], showing the dominant ( $A_{1g}$ ) gap function for  $n = 1.0$  and  $J/U = 0.3$ . (b) Two-dimensional contour plot of  $\chi_0$  also for  $n = 1.0$ . The horizontal (blue) vector in panel (a) connects the maximum amplitude of the gap function in *both* pockets. Note also the horizontal (blue) vector in panel (b) along the  $k_x$  direction, indicating the position of the maximum value of  $\chi_0$ . These two vectors agree up to a difference smaller than the width of this maximum peak in  $\chi_0$ . Therefore, it can be shown (see text) that the line describing the position of the points in the  $M$  pocket in relation to the points in the  $\Gamma$  pocket, as indicated by the two additional vectors (black and red) in panel (a), satisfies  $k_y \sim -k_x + k_n$ , where  $(k_n, 0)$  and  $(0, k_n)$  are the positions of the maxima in  $\chi_0$  (with  $n = 1.0$ ). This equation also describes the line of local maxima of  $\chi_0$ , as seen in panel (b), originating from FS nesting.

tangent to the hole pockets at the points where each intercepts the  $\Gamma - M$  ( $\Sigma$ ) line. As described in more detail in Fig. 5(a) [and already mentioned in connection with Fig. 1(a)], as the filling increases these segments of FS approach more and more the parallel lines just defined, justifying the definition just given.

The RPA results for the gap functions also point to an interesting effect, namely, the small value of  $\mathbf{k}_n$  for fillings  $0.46 \leq n \leq 1.0$  results in the pairing strength depending on very “local” properties of the gap function at the adjacent segments of the hole pockets. This implies that the pairing strength of gap functions with different symmetries is very similar, as long as they have the same local properties. To demonstrate that, in Fig. 4(a) the dominant gap function (with  $A_{1g}$  symmetry) is shown for  $n = 1.0$  and  $J/U = 0.3$ . It is clear that it is very similar in structure [near  $(\pi/2, \pi/2)$ ] to the  $B_{2g}$  ones shown in the previous figures. In the inset to Fig. 4(b) the subdominant gap function with symmetry  $B_{2g}$  is displayed for the same parameters. Note that comparing it with the dominant gap function in panel (a), despite having different symmetries, the two gap functions are *identical* in the two adjacent hole-pocket segments that cross the  $\Sigma$  line. For this reason, their pairing strengths as measured by  $\lambda$  (the eigenvalues of the Eliashberg equation), and shown in the main panel of Fig. 4(b), are the same to the third decimal place. Note that the two eigenvalues for symmetries  $A_{1g}$  and  $B_{2g}$  are *not* degenerate. This seems a strong indication that the local aspect of the pair scattering, as mentioned above, seems to be determinant to establish the pairing properties of this model, at least in our RPA weak-coupling approach. It should be noted that the eigenvalue results shown in Fig. 4 are basically identical to those for lower fillings, shown in previous figures, with the only difference being the order of the dominant and subdominant

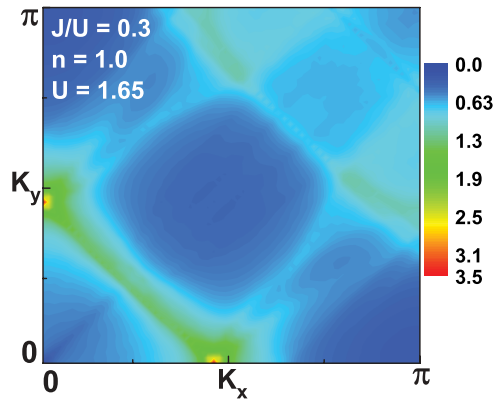


FIG. 6. (Color online) Two-dimensional plot of the RPA spin susceptibility for  $n = 1.0$ . The parameter values are  $J/U = 0.3$  and  $U = 1.65$ . The similarity to the results in Fig. 5(b) is clear, showing also that there are relevant nesting features along the  $k_y = -k_x + k_{1,0}$  line. Note that a smaller value of  $U$  than in Fig. 5(a) was used to avoid having a peak at  $(k_{1,0}, 0)$  that would wash out the features in the rest of the BZ.

symmetries. Since their eigenvalues are almost identical for all fillings studied, this switch in the order of the symmetries for  $n = 1.0$  does not seem to have a special significance. Note that  $\chi_{\text{RPA}}$  for  $n = 1.0$  and  $J/U = 0.3$  (not shown) follows the same trends as described in Figs. 2 and 3. From the orbital composition in Fig. 3(b) and the gap structure in Fig. 4 it appears that the symmetry of the  $B_{2g}$  and  $A_{1g}$  pairing operators is determined by the orbitals, while the spatial form in both cases is characterized by symmetric nearest-neighbor pairing with rotational invariance. Thus, the pairing operators have the form  $\Delta^\dagger = f(\mathbf{k})(d_{\mathbf{k},X,\uparrow}^\dagger d_{-\mathbf{k},X,\downarrow}^\dagger \pm d_{\mathbf{k},Y,\uparrow}^\dagger d_{-\mathbf{k},Y,\downarrow}^\dagger)$  where the  $+$  ( $-$ ) sign corresponds to  $A_{1g}$  ( $B_{2g}$ ) symmetry with  $f(\mathbf{k}) = \cos k_x + \cos k_y$ , plus higher harmonics with  $A_{1g}$  symmetry.

Figure 5(a) shows in more detail the almost parallel FS segments of the two hole pockets for  $n = 1.0$ . In this figure, the horizontal (blue) vector that was defined above as the separation between the two FS segments is displayed. A vector with the *same* length is reproduced in panel (b), where a 2D plot of  $\chi_0$  in the first quadrant of the BZ is also shown. It clearly indicates that the position  $\mathbf{k}_n$  of the main peak in  $\chi_0$  is *exactly* given by the horizontal separation. Not only that, the (red) vector along the  $\Sigma$  line in panel (a) is also reproduced in panel (b) and it too coincides exactly with a local maximum of  $\chi_0$ . In fact (see in both panels the black vectors located at angle  $\alpha$ ), the locus of the ridge of local maxima in  $\chi_0$  in panel (b) exactly coincides with the BZ points defined by the vectors connecting the two FS segments for  $0 \leq \alpha \leq \pi/2$ . Figure 6 shows the RPA spin susceptibility for  $n = 1.0$ . The similarity between these results and those in Fig. 5(b) is

clear, indicating that the FS nesting for the interacting system is the one described by the vectors in Fig. 5. Finally, an important issue should be highlighted: The four points in the hole pockets in Fig. 5(a) where the gap function has a very pronounced peak, are exactly the two pairs of points (one in each pocket) connected by  $(k_{1,0}, 0)$  and  $(0, k_{1,0})$ . This fact clearly links the pairing properties with the spin fluctuations. Note also that for  $n = 1.0$  and  $J/U = 0.3$ , the second pair of eigenvalues ( $\lambda_3 = 0.9038$  and  $\lambda_4 = 0.9036$ ) corresponds to symmetries  $A_{2g}$  and  $B_{1g}$ , respectively (not shown). The same occurs for  $J/U = 0.1$  and  $J/U = 0.2$ , also for  $n = 1.0$  (but the eigenvalues are smaller). Yet, the same explanation as described in Fig. 5 applies. See the Supplemental Material<sup>35</sup> for a connection between the emergence of a  $B_{1g}$  symmetry at  $n = 0.50$  with the one dimensionality of the bands.

*Conclusions.* Summarizing, a weak-coupling RPA analysis of a minimal 2-orbital model was used to investigate the pairing properties of the BiS<sub>2</sub>-based superconductors. Fillings between 0.46 and 1.0 were analyzed. The Hund's coupling was varied in the range  $0.1 \leq J/U \leq 0.4$ . Qualitatively, the results are similar for all values of  $J/U$  and different fillings. In the RPA results described here, a clear relationship is found between quasi-FS nesting, spin fluctuations, and superconductivity: The topology of the two hole pockets is such that they present almost parallel segments close to the  $(\pi/2, \pi/2)$  wave vector in the BZ. It is found that the horizontal distance  $(k_n, 0)$  between the tangents to these segments at the points where they cross the  $\Sigma$  line is also where the noninteracting susceptibility  $\chi_0$  has a pronounced peak at  $(k_n, 0)$ , for  $0.46 \leq n \leq 1.0$ . Once interactions are introduced, this peak will diverge at a certain critical coupling  $U$  for each filling, and all the values of  $J/U$  studied (with the exception of one:  $n = 0.5$ ,  $J/U = 0.1$ ). In addition, a line of local maxima, connecting the BZ points  $(k_n, 0)$  and  $(0, k_n)$ , is clearly observed in a 2D plot of  $\chi_0$ . As expected, this line can also be associated to FS nesting. This nesting structure gives origin to pairing functions with similar eigenvalues, i.e., similar pairing strengths, and symmetries  $B_{2g}$  and  $A_{1g}$ . This close competition originates in the FS quasineesting properties, which determine the spin-fluctuation-mediated interpocket pair scattering. This pair scattering is overwhelmingly between two adjacent FS segments, therefore the properties of the pairing functions, including the pairing strength, are quite local, having almost no dependence on their global symmetry. One can then predict that pairing symmetry measurements may contain a mixture of both symmetries if the pairing mechanism is driven by spin fluctuations.

*Acknowledgments.* G.B.M. acknowledges fruitful conversations with K. Kuroki, Q. Luo, and H. Usui. E.D. and A.M. were supported by the National Science Foundation Grant No. DMR-1104386.

\*Corresponding author: martins@oakland.edu

<sup>1</sup>Y. Mizuguchi, H. Fujihisa, Y. Gotoh, K. Suzuki, H. Usui, K. Kuroki, S. Demura, Y. Takano, H. Izawa, and O. Miura, *Phys. Rev. B* **86**, 220510(R) (2012).

<sup>2</sup>Y. Mizuguchi, S. Demura, K. Deguchi, Y. Takano, H. Fujihisa, Y. Gotoh, H. Izawa, and O. Miura, *J. Phys. Soc. Jpn.* **81**, 114725 (2012).

<sup>3</sup>H. Usui, K. Suzuki, and K. Kuroki, *Phys. Rev. B* **86**, 220501(R) (2012).

<sup>4</sup>S. Li, H. Yang, J. Tao, X. Ding, and H.-H. Wen, [arXiv:1207.4955](https://arxiv.org/abs/1207.4955).

<sup>5</sup>S. Demura, Y. Mizuguchi, K. Deguchi, H. Okazaki, H. Hara, T. Watanabe, S. Denholme, M. Fujioka, T. Ozaki, H. Fujihisa, Y. Gotoh, O. Miura, T. Yamaguchi, H. Takeya, and Y. Takano, [arXiv:1207.5248](https://arxiv.org/abs/1207.5248).

- <sup>6</sup>S. Tan, L. Li, Y. Liu, P. Tong, B. Zhao, W. Lu, and Y. Sun, *Physica C* **483**, 94 (2012).
- <sup>7</sup>S. Singh, A. Kumar, B. Gahtori, S. Kirtan, G. Sharma, S. Patnaik, and V. Awana, *J. Am. Chem. Soc.* **134**, 16504 (2012).
- <sup>8</sup>V. Awana, A. Kumar, R. Jha, S. Kumar, J. Kumar, A. Pal, J. Saha, and S. Patnaik, *Solid State Commun.* (2013), [arXiv:1207.6845](https://arxiv.org/abs/1207.6845).
- <sup>9</sup>H. Kotegawa, Y. Tomita, H. Tou, H. Izawa, Y. Mizuguchi, O. Miura, S. Demura, K. Deguchi, and Y. Takano, *J. Phys. Soc. Jpn.* **81**, 103702 (2012).
- <sup>10</sup>T. Zhou and Z. Wang, *J. Supercond. Nov. Magn.* (2013), [arXiv:1208.1101](https://arxiv.org/abs/1208.1101).
- <sup>11</sup>X. Wan, H.-C. Ding, S. Savrasov, and C.-G. Duan, [arXiv:1208.1807](https://arxiv.org/abs/1208.1807).
- <sup>12</sup>H. Takatsu, Y. Mizuguchi, H. Izawa, O. Miura, and H. Kadowaki, *J. Phys. Soc. Jpn.* **81**, 125002 (2012).
- <sup>13</sup>C. Sathish and K. Yamaura, [arXiv:1208.2818](https://arxiv.org/abs/1208.2818).
- <sup>14</sup>R. Jha, A. Kumar, S. Singh, and V. Awana, *J. Supercond. Nov. Magn.* (2013), [arXiv:1208.3077](https://arxiv.org/abs/1208.3077).
- <sup>15</sup>J. Xing, S. Li, X. Ding, H. Yang, and H.-H. Wen, *Phys. Rev. B* **86**, 214518 (2012).
- <sup>16</sup>S. Tan, P. Tong, Y. Liu, W. Lu, L. Li, B. Zhao, and Y. Sun, *Eur. Phys. J. B* **85**, 414 (2012).
- <sup>17</sup>R. Jha, S. Singh, and V. Awana, [arXiv:1208.5873](https://arxiv.org/abs/1208.5873).
- <sup>18</sup>K. Deguchi, Y. Mizuguchi, S. Demura, H. Hara, T. Watanabe, S. Denholme, M. Fujioka, H. Okazaki, T. Ozaki, H. Takeya, T. Yamaguchi, O. Miura, and Y. Takano, *Eur. Phys. Lett.* **101**, 17004 (2013).
- <sup>19</sup>B. Li and Z. Xing, *Eur. Phys. Lett.* (2013), [arXiv:1210.1743](https://arxiv.org/abs/1210.1743).
- <sup>20</sup>S. Liu, [arXiv:1210.2154](https://arxiv.org/abs/1210.2154).
- <sup>21</sup>A. Zhang and Q. Zhang, *Mod. Phys. Lett. B* **26**, 1230020 (2012).
- <sup>22</sup>H. Lei, K. Wang, M. Abeykoon, E. Bozin, and C. Petrovic, [arXiv:1208.3189](https://arxiv.org/abs/1208.3189).
- <sup>23</sup>Y. Kamihara, T. Watanabe, M. Hirano, and H. Hosono, *J. Am. Chem. Soc.* **130**, 3296 (2008).
- <sup>24</sup>G. R. Stewart, *Rev. Mod. Phys.* **83**, 1589 (2011).
- <sup>25</sup>P. Dai, J. Hu, and E. Dagotto, *Nat. Phys.* **8**, 709 (2012).
- <sup>26</sup>D. C. Johnston, *Adv. Phys.* **59**, 803 (2010).
- <sup>27</sup>Elbio Dagotto, [arXiv:1210.6501](https://arxiv.org/abs/1210.6501) [*Rev. Mod. Phys.* (to be published)].
- <sup>28</sup>T. Yildirim, [arXiv:1210.2418](https://arxiv.org/abs/1210.2418).
- <sup>29</sup>J. Lee, M. Stone, A. Huq, T. Yildirim, G. Ehlers, Y. Mizuguchi, O. Miura, Y. Takano, K. Deguchi, and S. Demura, [arXiv:1212.4811](https://arxiv.org/abs/1212.4811).
- <sup>30</sup>Although the experimentally relevant electron density is  $n \sim 0.5$ , the study of higher  $n$  values had the sole purpose of verifying the consistency of our results and interpretation for a larger set of qualitatively similar FS geometries to ascertain that the results did not depend fundamentally on some detail of the FS. Our results lead to the same interpretation for the full range of density values analyzed.
- <sup>31</sup>Note that in Ref. 3 [Fig. 4(c),  $n = 0.5$ ], there are small pockets around the  $(\pi, 0)$  points. To obtain these pockets, hopping matrix elements to considerably larger distances have to be added to the Hamiltonian considered here. The authors of Ref. 3 ascertained that the presence or not of these pockets does not alter the main RPA results (private communication).
- <sup>32</sup>Q. Luo, G. Martins, D.-X. Yao, M. Daghofer, R. Yu, A. Moreo, and E. Dagotto, *Phys. Rev. B* **82**, 104508 (2010).
- <sup>33</sup>S. Graser, T. A. Maier, P. J. Hirschfeld, and D. J. Scalapino, *New J. Phys.* **11**, 025016 (2009).
- <sup>34</sup>A. Nicholson, Q. Luo, W. Ge, J. Riera, M. Daghofer, G. B. Martins, A. Moreo, and E. Dagotto, *Phys. Rev. B* **84**, 094519 (2011).
- <sup>35</sup>See Supplemental Material at <http://link.aps.org/supplemental/10.1103/PhysRevB.87.081102> for RPA results in the spin-triplet channel, as well as an evaluation of the properties of an associated quasi-1d model.